Effect of Mg/B ratio on the superconductivity of MgB2 bulk with SiC addition

Yun Zhang
University of Wollongong, yunz@uow.edu.au

S X. Dou
University of Wollongong, shi@uow.edu.au

Cheng Lu
University of Wollongong, chenglu@uow.edu.au

Sihai Zhou
University of Wollongong, sihai@uow.edu.au

Wenxian Li
University of Wollongong, wenxian@uow.edu.au

Effect of Mg/B ratio on the superconductivity of MgB$_2$ bulk with SiC addition

Y. Zhang,[1] S. X. Dou,[1] C. Lu,[2] S. H. Zhou,[1] and W. X. Li[1]

[1]*Institute for Superconducting and Electronic Materials, University of Wollongong,*
Northfields Avenue, Wollongong, New South Wales 2522, Australia
[2]*School of Mechanical, Materials and Mechatronic Engineering, University of Wollongong,*
Northfields Avenue, Wollongong, New South Wales 2522, Australia

To improve the self-field critical current density (J_c) and critical temperature (T_c) in SiC-doped MgB$_2$, optimization of the nominal Mg/B mixing ratio has been performed. The effects of the nominal Mg/B mixing ratio (x:2) on the superconductivity, Raman spectra, current transport properties, and flux pinning mechanisms in MgB$_2$ with 10 wt.% SiC doping were investigated systematically, with x varied from 1 to 1.2. It has been found that the sample with the Mg/B ratio of 1.15:2 exhibited the best J_c performance for all fields (0–8.5 T), and its T_c was also enhanced. The optimized Mg/B ratio diminished the interband scattering caused by Mg or B vacancies, and in turn, increased T_c. The connectivity and disorder were increased in the Mg$_{1.15}$B$_2$ sample. Both of these were responsible for the improved J_c under all the fields examined.

I. INTRODUCTION

Since the 40 K superconductor MgB$_2$ was discovered in 2001,[1] the doping of nano-SiC particles into this superconductor has represented a great breakthrough in terms of improvement of the critical current density (J_c), the irreversibility field (H_{irr}), and the upper critical magnetic field (H_{c2}).[2–4] Worldwide, a number of groups have investigated and confirmed these results and reported an even further enhanced influence of SiC doping on MgB$_2$ properties. A record H_{irr} of 29 T and H_{c2} of 43 T at 4.2 K have been achieved with nano-SiC doped MgB$_2$.[4–6] J_c of 4.1×10^4 A/cm^2 at 4.2 K and 10 T has been achieved with nano-SiC doped MgB$_2$ wires.[7] However, there have been some drawbacks with this dopant, such as the reduction in the critical temperature (T_c) and the low-field J_c.

Optimization of the stoichiometry of Mg and B in undoped MgB$_2$ has been performed by many groups.[8–13] Both T_c and J_c showed great dependence on the Mg/B ratio. Susner *et al.*[8] have concluded that the Mg/B ratio significantly affects the microstructure, H_{irr}, and J_c. They also investigated the influence of SiC addition on the higher excess Mg compositions (around 15%). It has been found that 5 mol% SiC doping yielded a transport J_c at 4.2 K and 8 T of 5 $\times 10^4$ A/cm^2, with an H_{irr} of 21 T (100 A/cm^2 criterion). Recent results showed that a 10 wt.% Mg excess in the Mg-B system can improve the J_c values over the entire range (0–8.5 T) of measurement fields.[14] This has stimulated the idea that SiC doping in MgB$_2$ with Mg excess may be effective in improving the microstructure and J_c performance of MgB$_2$ in both low and high fields. Therefore, systematic studies on the effects of the nominal mixing ratio of Mg to B in SiC-doped MgB$_2$ are necessary and immediately important.

In this work, the effects of the nominal Mg/B ratio (x:2), varying from 1:2 to 1.2:2, in 10 wt.% SiC-doped MgB$_2$ samples on the superconductivity, Raman spectra, current transport properties, and flux pinning mechanisms of MgB$_2$ have been investigated systematically. The results show that

samples with 15 wt.% Mg excess in 10 wt.% SiC-doped MgB$_2$ exhibit the best performance. J_c has been improved at all the fields. The reason can be attributed to the improved connectivity and the increased disorder. Compared with other SiC-doped MgB$_2$ samples, T_c in the sample with 15 wt.% Mg excess has also been enhanced due to the increased electron-phonon (e-ph) coupling caused by the lower interband scattering.

II. EXPERIMENTAL DETAILS

It has been found that 10 wt.% SiC doping results in the best J_c performance.[2,15] Therefore, the doping concentration of SiC in this study was fixed at 10 wt.%. The nominal mixing ratio of Mg to B (x:2) varied from 1:2 to 1.2:2. Four Mg$_x$B$_2$ samples with x=1, 1.1, 1.15, and 1.2, mixed with 10 wt.% SiC, were prepared by solid state reaction. They are denoted as samples *A*, *B*, *C*, and *D* in the following context, respectively. A pure MgB$_2$ sample, made without dopant and by applying the same process, was also fabricated for comparison. It is defined as the reference sample. Mg powder (1–11 μm), amorphous boron powder (99%), and nano-sized crystalline SiC powder (30 nm) were used as the starting materials. The powders were carefully mixed by grinding in a mortar and pressed into pellets 13 mm in diameter and about 2.5 mm thick. The pellets were sealed into Fe tubes. The sealed tubes were then heated in a tube furnace under pure Ar gas and sintered at 800 °C for 60 h prior to cooling to room temperature.

The obtained MgB$_2$ samples were examined by x-ray diffraction (XRD) in a Philips PW1730 Model diffractometer using Cu Kα radiation (λ=1.541838 Å). The XRD patterns were collected over a 2θ range from 20° to 80° with a step size of 0.02°. Magnetic measurements of the samples were conducted in a commercial Quantum Design Physical Properties Measurement System (PPMS) after they had been polished into a cuboid shape for measurements. Magnetic hysteresis loops were measured at temperatures of 5 and 20 K. The critical current density was calculated from the magne-
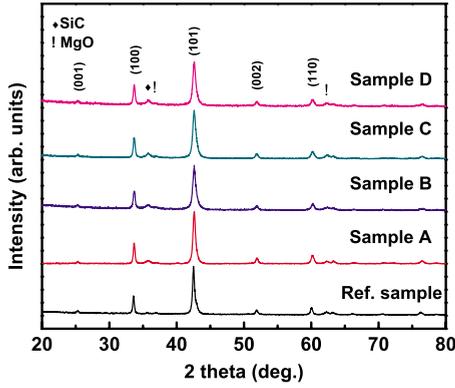
FIG. 1. (Color online) X-ray diffraction patterns for samples.

tization hysteresis loops, based on the dimensions of the samples. The resistivity was recorded as a function of temperature and magnetic field, using a four probe resistance technique. The Raman scattering was measured at ambient temperature by a confocal laser Raman spectrometer (Renishaw inVia plus) with a $100\times$ microscope. A 514.5 nm wavelength Ar+laser was used for excitation, with the laser power maintained at about 20 mW. Several spots were selected on the same sample to collect the Raman signals in order to make sure that the results were credible.

III. RESULTS AND DISCUSSION

Figure 1 shows the powder XRD patterns of the samples. All the major peaks of the MgB_2 hexagonal structure can be identified, indicating that the samples mainly consist of the desired MgB_2 phase. Besides MgB_2, the impurity MgO exists in all the samples. It is interesting to note that Mg_2Si, which was often observed in previous SiC-doped samples,[2–4] could not be detected in our SiC-doped samples (samples *A*, *B*, *C*, and *D*), while crystalline SiC clearly appears in the XRD patterns. The difference between the current samples and the previous samples is the form of the SiC powders. Amorphous SiC was used in the previous samples, whereas crystalline SiC was adopted in this study. The XRD pattern in Fig. 1 indicates that the crystalline SiC powder is not as active as the amorphous powder, in terms of reaction with MgB_2. Therefore, only a small amount of Mg_2Si, which may be below the detectable amount from XRD, was formed,

resulting in a large amount of remnant crystalline SiC in the samples.

Rietveld refinement was performed to analyze the XRD measurements. The refinable parameters included the lattice parameters of MgB_2 and the microstrain. The refined results are listed in Table I. The lattice parameters *a* and *c* decrease as *x* increases from 1 to 1.1, and then increase with *x* thereafter. The reference sample exhibits the highest value of *a*, while its *c* value is lower than for samples *C* and *D*. The values of the lattice parameters for ideal MgB_2 are *a* =3.083 Å and *c*=3.521 Å. It can be seen that lattice parameters *a* and *c* in the reference sample are greater than the ideal values. This indicates that a large amount of vacancies exist in the sample. The starting boron and magnesium powders in the reference sample were stoichiometrically mixed. The formation of MgO by the reaction of boron powder and oxygen trapped in the sealed tube and in the starting boron powders results in insufficient magnesium to react with boron. Mg may coat on the inner surface of the iron tube due to vaporization. This is another source of Mg loss. Since the tube is sealed, when the vapor pressure of Mg reaches a saturation value the Mg vaporization stops. Therefore, the Mg lose due to vaporization is limited. Deficiency of magnesium can be responsible for vacancies. The existence of the vacancies relaxes the lattice around them and increases both the *a* and *c* lattice parameters. As a result of SiC doping in sample *A*, lattice parameter *a* becomes smaller than for the reference sample, while lattice parameter *c* remains unchanged. Lattice parameter *a* in sample *A* is also smaller than the ideal value (a=0.083 Å). This indicates that C atoms have replaced part of the boron atoms. The C–B bond length is about 1.71 Å, which is less than the C–C bond length (1.78 Å).[16] Since the C–B bonds are located in the B plane, the in-plane lattice parameter *a* is decreased, whereas the distance between the B plane and the Mg plane, namely, lattice parameter *c*, would not be significantly affected. This phenomenon is often observed in MgB_2 samples with carbon doping.[17,18] As the mixing ratio of Mg to B ($x:2$) increases to 1.1:1, the deficiency of magnesium is reduced. This decreases the lattice relaxation caused by the magnesium deficiency and further reduces lattice parameter *a* in $Mg_{1.1}B_2$. However, when *x* is over 1.15, the magnesium deficiency is completely healed, and boron deficiency will be introduced. The boron deficiency also relaxes the lattice and increases *a*. It has been observed that *a* is enlarged when *x* increases to

TABLE I. Calculated refinable parameters.

| Samples | Nominal stoichiometry | Lattice parameters | | | Strain (%) | | |
		a (Å)	c (Å)	Volume (Å³)	a axis	c axis	Average
Reference	MgB_2	3.087	3.526	29.10	0.345	0.548	0.447
A	MgB_2+10%SiC	3.081	3.526	28.99	0.392	0.628	0.510
B	$Mg_{1.1}B_2$+10%SiC	3.079	3.525	28.94	0.490	0.835	0.663
C	$Mg_{1.15}B_2$+10%SiC	3.082	3.527	29.01	0.461	0.812	0.647
D	$Mg_{1.2}B_2$+10%SiC	3.087	3.532	29.15	0.463	0.694	0.579

TABLE II. Properties of samples.

Samples	T_c (K)	$\rho_{40 \text{ K}}$ ($\mu\Omega$ cm)	$\rho_{300 \text{ K}}$ ($\mu\Omega$ cm)	A_F	J_c (20 K, 0 T) (A cm^{-2})	J_c (20 K, 5 T) (A cm^{-2})	κ (20 K)
Reference	37.54	58.6	104.6	0.159	231756	868.4	20.3
A	35.42	128.7	206.5	0.094	201336	2144.3	20.4
B	35.75	99.4	149.0	0.147	242403	3125.5	20.5
C	36.25	76.4	118.7	0.173	326057	4729.0	19.5
D	35.70	94.2	143.6	0.148	309326	3633.7	18.4

1.2. The effect of the boron deficiency on a in sample D even compensates for the decrease in a caused by the C substitution. Therefore, lattice parameter a in sample D is similar to a for the reference sample. In addition, the excess Mg in sample D may be squeezed between the B plane and the Mg plane. Therefore, a significant increase in lattice parameter c can be observed in sample D. The unit-cell volume of MgB$_2$ is calculated according the refined lattice parameters a and c, and is listed in Table I. It can be seen that the reference sample has a larger unit-cell volume than the doped samples, except for sample D. Among the doped samples, sample B has the smallest volume.

The microstrains along the two lattice axes (a and c) are shown in Table I. The microstrains in the samples exhibit anisotropic behavior, namely, the microstrain along the c axis is larger than that along the a axis. The anisotropic microstrain is caused by the anisotropic elastic modulus along the different axes. The smaller elastic modulus along the c axis results in a larger strain.[19] The average values are obtained by arithmetically averaging the values along the two lattice axes. As expected, the doped samples have larger microstrain than the reference sample due to C substitution. When x increases, the average microstrain increases from sample A to sample B, and then decreases. This indicates that the nominal Mg/B ratio significantly affects the microstrain.

The magnetic susceptibility as a function of temperature was measured in an applied field of $H=1$ Oe for zero field cooled samples. T_c is defined as the temperature corresponding to the onset of diamagnetism. The T_c values are displayed in Table II. It can be seen that the reference sample has the largest T_c. As x increases in the doped samples, T_c increases from sample A to sample C, and then decreases in sample D. Sample C with $x=1.15$ exhibits the largest T_c among the doped samples.

In order to analyze the origin of the variation in T_c, Raman measurements were undertaken. Figure 2 contains the normalized ambient Raman spectra of all the samples. Gaussian fittings with three peaks are also shown in Fig. 2. The ω_1, ω_2, and ω_3 peaks are centered at about 399.1–409.3 cm^{-1}, 568.9–597.9 cm^{-1}, and 702.1–779.3 cm^{-1}, respectively. First principles calculations[20–22] indicated that the high T_c of MgB$_2$ is due to the electron-phonon (e-ph) coupling between the in-plane boron phonons (E_{2g} mode) and the σ band. The Raman spectra of MgB$_2$ around 600 cm^{-1}, namely, the ω_2 peak in Fig. 2, have been attributed to the E_{2g} mode.[23] The ω_2 peak frequencies are extracted and plotted against x in Fig. 3. It is clear that the reference sample has a lower ω_2 peak frequency than the doped samples. This can be attributed to the carbon substitution caused by the SiC doping. It is well known that the charge carriers in MgB$_2$ are holes. The carbon substitution introduces more electrons and therefore reduces the number of holes. This hole-filling effect weakens the e-ph coupling. Theoretical analysis has concluded that the E_{2g} peak frequency increases as the e-ph coupling becomes weaker.[24] Therefore, the doped samples in this study exhibit higher ω_2 peak frequencies than the reference sample. The same observations have been reported for C-doped and Al-doped MgB$_2$.[16,25,26]

It can be seen from Fig. 3 that the ω_2 peak frequency decreases as x rises from 1 to 1.15, and then increases for $x=1.2$. Since all the doped samples have the same doping
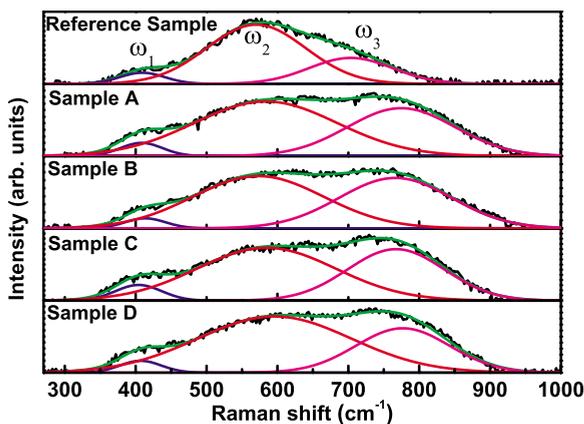
FIG. 2. (Color online) Normalized Raman spectra with three-peak Gaussian fitting.
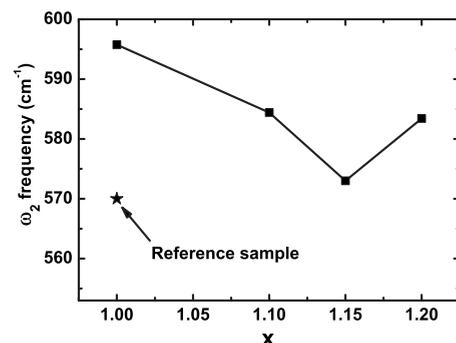
FIG. 3. ω_2 peak frequency against x.

concentration (10 wt.%) of SiC, the hole-filling effects should be similar. An additional effect causing the variation of the ω_2 peak frequency may be the interband scattering.[27] There are two major factors affecting the interband scattering: lattice parameters and defects. The σ band is located in the boron plane, while the π band is also centered in the boron plane and extends out towards the Mg plane. Therefore, lattice parameter a in the boron plane influences the interband scattering. A decreased lattice parameter a will increase the interband scattering. This will harden the E_{2g} phonon and weaken the e-ph coupling. From Table I we can see that lattice parameter a first decreases with x and then increases. This will cause the ω_2 frequency to increase first and then decrease. However, this trend is opposite to the observed ω_2 peak frequencies in Fig. 3. This implies that there is another factor playing a more important role in the interband scattering than lattice parameter a. The major defects in the studied samples are the vacancies caused by Mg deficiency and B deficiency. An increase in the amount of vacancies will reduce the interband scattering and harden the E_{2g} phonon. It is well known that the vacancy defects decrease with x for low mixing ratios due to healing of the Mg deficiency and increase with x for high mixing ratios owing to formation of a B deficiency. Therefore, as x increases, the effect of the vacancy defects depresses the ω_2 frequency to the minimum and then increases it. Figure 3 shows that the measured ω_2 frequency follows the same trend as the effect of the vacancy defects. This indicates that the vacancy defects caused by Mg deficiency and B deficiency provide a greater contribution to the interband scattering than lattice parameter a.

For the strong electron-phonon coupling superconductors, T_c can be predicted by the McMillan equation,[28] as modified by Allen and Dynes[29]

$$T_c = \frac{\langle\omega\rangle}{1.2}\exp\left(\frac{-1.04(1+\lambda)}{\lambda - \mu^*(1+0.62\lambda)}\right), \qquad (1)$$

where, $\langle\omega\rangle$ is the averaged phonon frequency, λ is the e-ph coupling constant, and μ^* is the Coulomb pseudopotential. It can be seen from Eq. (1) that T_c increases with both $\langle\omega\rangle$ and λ for the commonly used μ^* of about 0.13 in MgB$_2$.[30] In addition, it is well known that $\langle\omega\rangle$ decreases as λ increases.[31] Thereby, if the e-ph coupling is strengthened, namely, λ is increased, $\langle\omega\rangle$ will be correspondingly reduced. The increased λ and the decreased $\langle\omega\rangle$ have opposite effects on T_c. The former enhances T_c, while the latter depresses T_c. Therefore, T_c will increase to the maximum and then decreases as the e-ph coupling (λ) increases. However, the λ value (about 2) corresponding to the maximum T_c is higher than the common range of λ (0.7–1.0) in MgB$_2$.[19–21] This leads to a monotonic increase of T_c with λ in the MgB$_2$ system. The e-ph coupling in the SiC-doped samples is weaker than in the reference sample due to the carbon substitution. Therefore, the reference sample has the highest T_c. In the doped samples, the vacancy defects significantly affect the e-ph coupling strength. Sample C with fewer vacancies yields a higher e-ph coupling constant, resulting in enhancement of T_c.
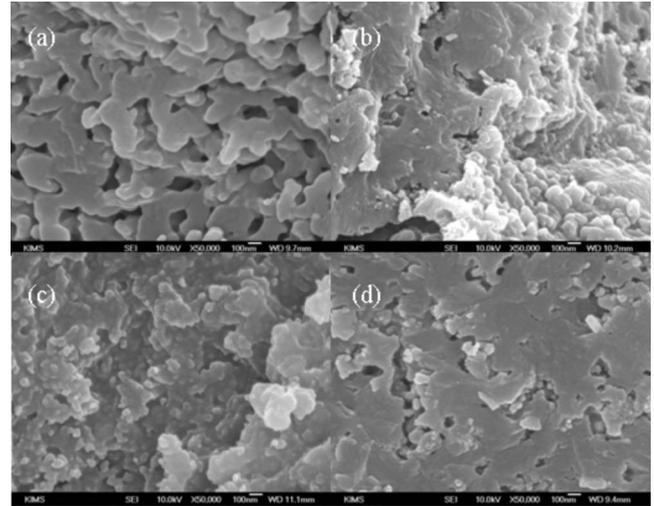
FIG. 4. Gun scanning electron microscope (FEG-SEM) images: (a) sample A; (b) sample B; (c) sample C; (d) sample D.

The resistivities at 40K ($\rho_{40\ K}$) and at 300K ($\rho_{300\ K}$) are listed in Table II. It can be seen that $\rho_{40\ K}$ and $\rho_{300\ K}$ in the reference sample are smaller than in the SiC-doped samples, while sample A with $x=1$ exhibits the highest $\rho_{40\ K}$ and $\rho_{300\ K}$. The resistivities decrease as x increases up to 1.15. When x further increases from 1.15 to 1.2, $\rho_{40\ K}$ and $\rho_{300\ K}$ are enhanced. All the $\rho_{40\ K}$ values listed in Table II are higher than for single crystal (5.3 $\mu\Omega$ cm)[32] and for dense filaments made by chemical vapor deposition (CVD) (7.3 $\mu\Omega$ cm).[33] This is due to poor connectivity in our samples. The effective cross-sectional area (A_F) can be estimated from the equation, $A_F = \Delta\rho_{ideal}/(\rho_{300\ K}-\rho_{40\ K})$, which was proposed by Rowell.[34] $\Delta\rho_{ideal}$ is the ideal change in resistivity from 300 to 40 K for a fully connected sample. It is set to be 7.3 $\mu'\Omega$ cm, according to Ref. 35. The calculated A_F is displayed in Table II. It can be seen that the A_F values are below 0.18, indicating poor connection in the samples. The poor connectivity is responsible for high resistivity. Sample A has the smallest A_F, while sample C exhibits the highest value. Figure 4 shows field emission gun scanning electron microscope (FEG-SEM) images. It can be seen that sample C is denser than the other samples. This confirms that sample C has the best connectivity. The densities in the reference sample and in samples A to D are 1.365, 1.313, 1.374, 1.393, and 1.246 g/cm^{-2}, respectively. Higher density means better connectivity. The density measurements also support the above estimation of the connectivity. MgB$_2$ is formed by diffusion of Mg atoms into the boron lattices. Since the impurities profoundly influence the Mg diffusion, the crystallization and connectivity are strongly related to the amount of impurities. The SiC doping in sample A introduced a large amount of impurities, such as remnant SiC, as shown in Fig. 1, and the consequent formation of Mg$_2$Si. Therefore, compared to the reference sample, the connectivity in sample A is reduced. Both the reference sample and sample A use the stoichiometric Mg/B ratio (1:2). This inevitably introduces remnant B due to the formation of MgO. The leftover B constitutes an impurity in MgB$_2$ and will degrade the connectivity. As the nominal Mg/B ratio in-
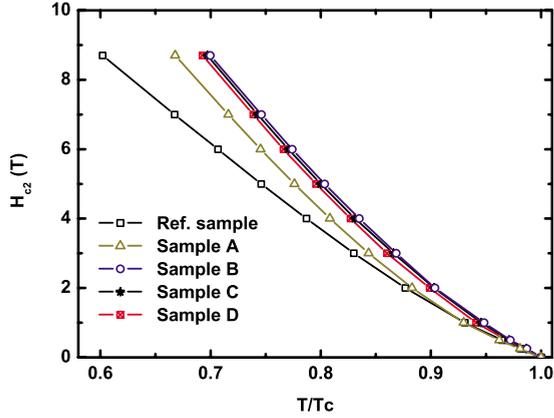
FIG. 5. (Color online) Temperature dependence of H_{c2}.

FIG. 7. (Color online) Critical current density $J_c(H)$ at 5 and 20 K.

creases, remnant B is reduced, leading to improved connectivity in samples B and C. When the nominal Mg/B ratio is further increased, the sample ceases to be B rich and becomes Mg rich, as appears in $Mg_{1.2}B_2$. The remnant Mg impurity in this sample decreases the connectivity, as indicated by A_F in Table II.

Figure 5 demonstrates the temperature dependence of the resistive upper critical magnetic field, H_{c2}, which is defined by 90% of the normal state resistivity. It can be seen that H_{c2} has a concave temperature-dependence curve, which is typical for multiband superconductors.[36,37] As the temperature increases, H_{c2} decreases. The reference sample has the lowest H_{c2}. When SiC is doped into MgB_2, H_{c2} is significantly increased. The nominal Mg/B ratio $(x:2)$ also influences H_{c2}. H_{c2} rises from sample A to sample B. Samples B, C, and D have similar H_{c2} values, and H_{c2} slightly decreases with x.

H_{c2} differences in the samples can be attributed to the variation in the coherence length (ξ) that is caused by the disorder. Figure 6 shows H_{c2} at $T/T_c = 0.7$ against microstrain. The solid line is the trend line. It is clear that H_{c2} increases with microstrain. A low microstrain indicates less disorder inside the MgB_2 grains and thus a larger mean free path (l) of the superconducting electrons. This will increase the coherence length (ξ) due to the relation: $\xi^{-1} = \xi_0^{-1} + l^{-1}$, where ξ_0 is the value of ξ for the pure superconductor. According to $H_{c2} = \Phi_0/(2\pi\mu_0\xi^2)$, where Φ_0 is the supercon-

FIG. 6. (Color online) H_{c2} against average microstrain and $I_{\omega3}/I_{\omega2}$.

ducting flux quantum and μ_0 is the magnetic permeability, H_{c2} decreases with increasing ξ. Therefore, a larger H_{c2} is caused by increased disorder. Figure 6 also plots H_{c2} as a function of the intensity ratio of the ω_3 peak to the ω_2 peak $(I_{\omega3}/I_{\omega2})$, which is extracted from Fig. 2. The dashed line represents its trend line. It can be seen that H_{c2} linearly increases with $I_{\omega3}/I_{\omega2}$. $I_{\omega3}/I_{\omega2}$ is another indicator of disorder. A larger $I_{\omega3}/I_{\omega2}$ means higher disorder. The plot of H_{c2} against $I_{\omega3}/I_{\omega2}$ in Fig. 6 confirms that the enhanced H_{c2} is due to the increased disorder.

J_c was calculated from the measured magnetization hysteresis loops, with the calculation based on the Bean model. J_c values at 5 and 20 K are shown in Fig. 7. At 5 K under low fields, flux jumping exists, as has been explained in the literature.[38] J_c in the flux jumping region is not shown in the figure. At 5 K and high fields, the reference sample has lower J_c than the doped samples, while in the doped samples, J_c increases with x up to 1.15 and decreases as x increases from 1.15 to 1.2. J_c values at 20 K at 0 T and 5 T are listed in Table II. Compared to the reference sample, sample A ($x = 1$) shows an increase in J_c by a factor of 2.5 for high field (5 T), while the self-field J_c of A is lower than for the reference sample. In Mg-rich samples ($x \geq 1.1$) J_c can be simultaneously increased for both low fields and high fields. The optimum Mg/B ratio is 1.15:2 in sample C. J_c of sample C at 20 K and 5 T is higher than for sample A by a factor of 2.3, while its self-field J_c is higher than for the reference sample by a factor of 1.4. These results clearly show that optimization of the nominal Mg/B mixing ratio can significantly increase J_c for all fields.

It is well known that grain boundary pinning is the major pinning mechanism at high fields in MgB_2. The J_c caused by the surface pinning can be calculated by $\frac{\mu_0 S_v (H_{c2}-H)^2}{4\kappa^2 H_{c2}^{1/2} H^{1/2}}$,[39] where S_v is the grain boundary surface area per unit volume, κ the Ginzburg-Landau parameter, and H the applied field. In addition, J_c is also proportional to the connectivity.[40] To describe the total influence of H_{c2}, κ, and A_F on J_c at high fields, we define a combined parameter $\alpha_1 = A_F \frac{(H_{c2}-H)^2}{\kappa^2 H_{c2}^{1/2}}$ for $H = 5$ T. Since it is difficult to determine κ due to the two-band contribution, we calculated an effective κ instead of the real κ by solving the equation: $\frac{\ln(\kappa)+0.5}{2\kappa^2} = \frac{H_{c1}}{H_{c2}}$.[40] H_{c2} was obtained by extrapolating the curves in Fig. 5 to $T_c = 20$ K, and H_{c1} was measured as the field at which the magnetic hysteresis curve starts to deviate from linearity. The calculated ef-
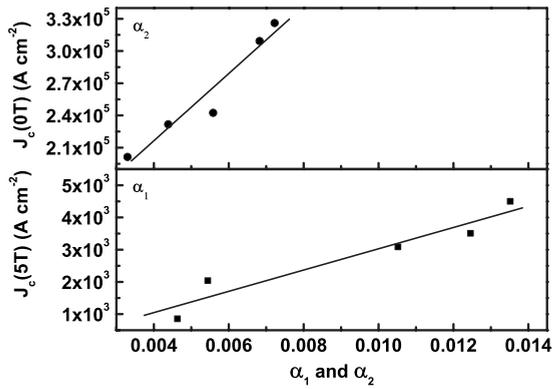
FIG. 8. J_c at 20 K and 5 T against α_1 (bottom panel), and J_c at 20 K and 0 T against α_2 (top panel).

fective κ values are shown in Table II. κ follows the same trend as the microstrain. This implies that κ is also affected by disorder. J_c at 20 K and 5 T versus α_1 is shown in the bottom panel of Fig. 8. A linear relationship can be observed. J_c (20 K, 5 T) increases with α_1. At self-field, the interflux-line spacing (d) tends to infinity. According to the Dew-Hughes model,[39] all defects act as point pinning centers at zero field, and the self-field J_c linearly increases with H_{c2} and decreases with κ^2. The self-field J_c is also proportional to the connectivity.[40] We define another combined parameter: $\alpha_2 = A_F \frac{H_{c2}}{\kappa^2}$, to represent the total influence of H_{c2}, κ, and A_F on the self-field J_c. The self-field J_c, J_{c0}, at 20 K is shown against α_2 in the top panel of Fig. 8. J_{c0} linearly increases with α_2. From the above analysis we can see that J_c is mainly affected by disorder and connectivity. The former influences J_c via H_{c2} and κ. As disorder increases, both H_{c2} and κ increase. However, the increased H_{c2} and the increased κ change J_c in opposite directions. J_c increases with H_{c2} and decreases with κ. Since the magnitude of variation of H_{c2} in the studied samples is larger than that of κ, H_{c2} plays a more important role in J_c than κ. The above analysis also shows that H_{c2} affects the high-field J_c and the self-field J_c by different factors. The high-field J_c is proportional to H_{c2} by $J_c \propto H_{c2}^{3/2}$, while the self-field J_c is proportional by $J_c \propto H_{c2}$. It is clear that H_{c2} has more impact on the high-field J_c than on the self-field J_c. Although sample A has lower connectivity than the reference sample, its higher H_{c2} can increase the high-field J_c over the value for the reference sample. Due to the lesser influence of H_{c2} on the self-field J_c, H_{c2} in sample A is not high enough to induce its self-field J_c to exceed J_{c0}

in the reference sample. This is the reason why a crossover has been observed between the J_c curves of the reference sample and sample A. As the Mg excess is increased, the connectivity is improved until $x=1.15$, while H_{c2} increases and reaches its maximum at $x=1.1$. The increased connectivity and H_{c2} will enhance J_c for all fields. Sample C has the best connectivity, and its H_{c2} is just slightly lower than the maximum value in sample B. Therefore, sample C exhibits the best performance of J_c for both low fields and high fields. It is more interesting to note that sample C also hosts an enhanced T_c. The combination of these excellent superconducting properties in sample C should clearly be attributed to optimization of the nominal Mg/B ratio. The optimized Mg/B ratio of 1.15:2 significantly reduces the vacancies caused by Mg deficiency and B deficiency, and correspondingly reduces the remnant B or remnant Mg. This leads to lower interband scattering and higher connectivity. Therefore, T_c and J_c for all the fields can be simultaneously improved. In addition, the doped SiC still remains in the samples with a high level of disorder, resulting in a high H_{c2} and J_c.

IV. CONCLUSION

In this paper, we systematically studied the effects of the nominal Mg/B mixing ratio (x:2) on the superconductivity, Raman spectra, current transport properties, and flux pinning mechanism in MgB$_2$ with 10 wt.% SiC doping. x was varied from 1 to 1.2. It has been seen that compared to MgB$_2$ without doping, the SiC-doped sample with the stoichiometric nominal Mg/B ratio (1:2) has significantly increased J_c at high fields. However, its self-field J_c and T_c were depressed. Through the optimization of the nominal Mg/B ratio, we found that the sample with $x=1.15$ exhibited the best J_c performance for all the fields (0–8.5 T), including the self-field, and its T_c was higher than for the sample with $x=1$. The enhancement of J_c is attributed to the improved connectivity and the increased disorder, both of which were achieved by the optimization of the Mg/B ratio. The optimized Mg/B ratio (1.15:2) also diminished the interband scattering caused by the Mg or B vacancies and in turn, increased T_c.

[1] J. Nagamatsu, N. Nakagawa, T. Muranaka, Y. Zenitani, and J. Akimitsu, Nature (London) **410**, 63 (2001).

[2] S. X. Dou, S. Soltanian, J. Horvat, X. L. Wang, S. H. Zhou, M. Ionescu, H. K. Liu, P. Munroe, and M. Tomsic, Appl. Phys. Lett. **81**, 3419 (2002).

[3] S. X. Dou, V. Braccini, S. Soltanian, R. Klie, Y. Zhu, S. Li, X. L. Wang, and D. Larbalestier, J. Appl. Phys. **96**, 7549 (2004).

[4] S. X. Dou, O. Shcherbakova, W. K. Yeoh, J. H. Kim, S. Solta-

nian, X. L. Wang, C. Senatore, R. Flukiger, M. Dhalle, O. Husnjak, and E. Babic, Phys. Rev. Lett. **98**, 097002 (2007).

[5] A. Matsumoto, H. Kumakura, H. Kitaguchi, B. J. Senkowicz, M. C. Jewell, E. E. Hellstrom, Y. Zhu, P. M. Voyles, and D. C. Larbalestier, Appl. Phys. Lett. **89**, 132508 (2006).

[6] M. D. Sumption, M. Bhatia, M. Rindfleisch, M. Tomsic, S. Soltanian, S. X. Dou, and E. W. Collings, Appl. Phys. Lett. **86**, 092507 (2005).

[7] K. Togano, T. Nakane, H. Fujii, H. Takeya, and H. Kumakura, Supercond. Sci. Technol. **19**, L17 (2006).

[8] M. A. Susner, M. D. Sumption, M. Bhatia, X. Peng, M. J. Tomsic, M. A. Rindfleisch, and E. W. Collings, Physica C **456**, 180 (2007).

[9] R. A. Ribeiro, S. L. Bud'ko, C. Petrovic, and P. C. Canfield, Physica C **382**, 194 (2002).

[10] D. G. Hinks, J. D. Jorgensen, H. Zheng, and S. Short, Physica C **382**, 166 (2002).

[11] C. H. Jiang and H. Kumakura, Physica C **451**, 71 (2007).

[12] H. Xiao, W. Peng, W. H. Song, R. C. Ma, L. Zhang, J. J. Du, and Y. P. Sun, Physica C **386**, 648 (2003).

[13] S. K. Chen, A. Serquis, G. Serrano, K. A. Yates, M. G. Blamire, D. Guthrie, J. Cooper, H. Wang, S. Margadonna, and J. L. MacManus-Driscoll, Adv. Funct. Mater. **18**, 113 (2008).

[14] R. Zeng, L. Lu, J. L. Wang, J. Horvat, W. X. Li, D. Q. Shi, S. X. Dou, M. Tomsic, and M. Rindfleisch, Supercond. Sci. Technol. **20**, L43 (2007).

[15] S. Soltanian, X. L. Wang, J. Horvat, S. X. Dou, M. D. Sumption, M. Bhatia, E. W. Collings, P. Munroe, and M. Tomsic, Supercond. Sci. Technol. **18**, 658 (2005).

[16] A. H. Moudden, J. Phys. Chem. Solids **67**, 115 (2006).

[17] S. Lee, T. Masui, A. Yamamoto, H. Uchiyama, and S. Tajima, Physica C **397**, 7 (2003).

[18] S. M. Kazakov, R. Puzniak, K. Rogacki, A. V. Mironov, N. D. Zhigadlo, J. Jun, Ch. Soltmann, B. Batlogg, and J. Karpinski, Phys. Rev. B **71**, 024533 (2005).

[19] A. K. M. A. Islam and F. N. Islam, Physica C **363**, 189 (2001).

[20] J. Kortus, I. I. Mazin, K. D. Belashchenko, V. P. Antropov, and L. L. Boyer, Phys. Rev. Lett. **86**, 4656 (2001).

[21] J. M. An and W. E. Pickett, Phys. Rev. Lett. **86**, 4366 (2001).

[22] Y. Kong, O. V. Dolgov, O. Jepsen, and O. K. Andersen, Phys. Rev. B **64**, 020501 (2001).

[23] K. P. Bohnen, R. Heid, and B. Renker, Phys. Rev. Lett. **86**, 5771 (2001).

[24] W. L. McMillan, Phys. Rev. **167**, 331 (1968).

[25] T. Masui, S. Lee, and S. Tajima, Phys. Rev. B **70**, 024504 (2004).

[26] D. Di Castro, E. Cappelluti, M. Lavagnini, A. Sacchetti, A. Palenzona, M. Putti, and P. Postorino, Phys. Rev. B **74**, 100505 (2006).

[27] I. I. Mazin, O. K. Andersen, O. Jepsen, O. V. Dolgov, J. Kortus, A. A. Golubov, A. B. Kuz'menko, and D. van der Marel, Phys. Rev. Lett. **89**, 107002 (2002).

[28] P. B. Allen and R. C. Dynes, Phys. Rev. B **12**, 905 (1975).

[29] M. Calandra, A. N. Kolmogorov, and S. Curtarolo, Phys. Rev. B **75**, 144506 (2007).

[30] A. Brinkman, A. A. Golubov, H. Rogalla, O. V. Dolgov, J. Kortus, Y. Kong, O. Jepsen, and O. K. Andersen, Phys. Rev. B **65**, 180517(R) (2002).

[31] J. Kortus, O. V. Dolgov, R. K. Kremer, and A. A. Golubov, Phys. Rev. Lett. **94**, 027002 (2005).

[32] Y. Eltsev, S. Lee, K. Nakao, N. Chikumoto, S. Tajima, N. Koshizuka, and M. Murakami, Phys. Rev. B **65**, 140501(R) (2002).

[33] P. C. Canfield, D. K. Finnemore, S. L. Bud'ko, J. E. Ostenson, G. Lapertot, C. E. Cunningham, and C. Petrovic, Phys. Rev. Lett. **86**, 2423 (2001).

[34] J. M. Rowell, Supercond. Sci. Technol. **16**, R17 (2003).

[35] J. Jiang, B. J. Senkowicz, D. C. Larbalestier, and E. E. Hellstrom, Supercond. Sci. Technol. **19**, L33 (2006).

[36] A. A. Golubov and A. E. Koshelev, Phys. Rev. B **68**, 104503 (2003).

[37] A. E. Koshelev and A. A. Golubov, Phys. Rev. Lett. **92**, 107008 (2004).

[38] B. Seeber, *Handbook of Applied Superconductivity* (Institute of Physics, Bristol, UK, 1998), Vol. 1.

[39] D. Dew-Hughes, Philos. Mag. **30**, 293 (1974).

[40] M. Eisterer, Supercond. Sci. Technol. **20**, R47 (2007).